Chemical Bonding in Si_5^{2-} and $NaSi_5^-$ via Photoelectron Spectroscopy and ab Initio Calculations†

Dmitry Yu. Zubarev and Alexander I. Boldyrev*

Department of Chemistry and Biochemistry, Utah State University, Logan, Utah 84322-0300

Xi Li, Li-Feng Cui, and Lai-Sheng Wang*

Department of Physics, Washington State University, 2710 University Drive, Richland, Washington 99356, and W. R. Wiley Environmental Molecular Sciences Laboratory and Chemical Sciences Division, Pacific Northwest National Laboratory, MS K8-88, P.O. Box 999, Richland, Washington 99352

Received: May 21, 2005; In Final Form: August 20, 2005

Photoelectron spectroscopy and ab initio calculations are used to investigate the electronic structure and chemical bonding of Si_5^- and Si_5^{2-} in $NaSi_5^-$. Photoelectron spectra of Si_5^- and $NaSi_5^-$ are obtained at several photon energies and are compared with theoretical calculations at four different levels of theory, TD-B3LYP, R(U)OVGF, UCCSD(T), and EOM-CCSD(T), all with 6-311+G(2df) basis sets. Excellent agreement is observed between experiment and theory, confirming the obtained ground-state structures for Si_5^- and Si_5^{2-}, which are both found to be trigonal bipyramid with D_{3h} symmetry at several levels of theory. Chemical bonding in Si_5, Si_5^-, and Si_5^{2-} is analyzed using NPA, molecular orbitals, ELF, and NICS indices. The bonding in Si_5^{2-} is compared with that in the isoelectronic and isostructural $B_5H_5^{2-}$ species, but they are found to differ due to the involvement of electron densities, which are supposed to be lone pairs in the skeletal bonding in Si_5^{2-}.

1. Introduction

The discovery of the C_{60} buckyball[1] has generated a great deal of interest in cagelike clusters, particularly in silicon clusters. However, the obvious valence isoelectronic Si_{60} analogue does not have the same structure as C_{60}.[2−9] Instead of a beautiful soccer-ball shape, Si_{60} seems to adopt a rather low symmetry structure.[2,4,7,9] An alternative approach to searching for cagelike silicon clusters is to use the isolobal analogy between an HB unit and a Si atom[10] and the known fact that boranes, such as $B_{12}H_{12}^{2-}$, have cagelike deltahedral structures.[11−13] However, our preliminary ab initio calculations of the Si_{12}^{2-} cluster[14] indicate indeed that an icosohedral Si_{12}^{2-} cage is a local minimum, although it is not the global minimum. Our preliminary results on other Si_x^{2-} clusters[14] also demonstrate that many doubly charged silicon anionic clusters adopt low-symmetry structures rather than the beautiful deltahedral structures. We are interested in developing a unified chemical bonding picture for silicon clusters and understanding the deviation of the geometric structures of doubly charged silicon cluster anions from the isolobal deltahedral $B_xH_x^{2-}$ analogues.[11−13]

We begin this endeavor with the Si_5^{2-} dianionic cluster, which has been recently synthesized and characterized in the solid state.[15] The Si_5^{2-} cluster was synthesized in the (Rb-crypt)$_2$Si$_5$-4NH$_3$ crystal and was shown to be a trigonal-bipyramidal cluster with equatorial distances $d_{eq-eq} = 2.535$ Å and axial distances $d_{ax-eq} = 2.350$ Å. An isolated Si_5^{2-} dianion is expected to be metastable toward autodetachment in the gas phase, but it may be stabilized by an alkali metal cation (M^+) in MSi_5^-. Kishi et al.[16] reported experimental observation of $NaSi_5^-$, as well as its photoelectron spectrum at 355 nm, which displayed one broad spectral band. They also presented theoretical calculations for $NaSi_5^-$ and Si_5^{2-} at the MP2/6-31G* level of theory and found a trigonal-bipyramidal structure for Si_5^{2-} and two isomers for $NaSi_5^-$: a C_{2v} ($^1A_1$) structure and a C_{3v} ($^1A_1$) structure. The C_{2v} structure with the Na^+ cation coordinated to the edge of the triangular base was found to be more stable by 0.823 eV (at MP4/6-31G*//MP2/6-31G*) than the C_{3v} isomer, in which the Na^+ cation was coordinated to one apex Si atom of the trigonal-bipyramidal Si_5^{2-} structure. The series of ME_5^- (M = Li, Na, K, and E = Si and Ge) anions have been studied by Li and co-workers,[17,18] who optimized the geometry for the trigonal-bipyramidal Si_5^{2-} structure using six different levels of theory. At their best density functional level of theory (B3PW91/6-311+G(3d2f)), they obtained $d_{ax-eq} = 2.53$ Å and $d_{eq-eq} = 2.75$ Å, and at their best ab initio level of theory (MP2/6-311G*) they got $d_{ax-eq} = 2.57$ Å and $d_{eq-eq} = 2.76$ Å. Both are in reasonable agreement with the Si_5^{2-} structure in the solid state: $d_{ax-eq} = 2.48$ Å and $d_{eq-eq} = 2.69$ Å.

In the current paper, we present a systematic and comprehensive study of Si_5^{2-} and $NaSi_5^-$ using a combined experimental and theoretical approach. Photoelectron spectra of $NaSi_5^-$ have been obtained at three photon energies: 355, 266, and 193 nm. The higher photon energy spectra yielded higher binding energy detachment features, which are better suited for comparison with the theoretical results. Molecular orbital analyses have been carried out to understand the detailed chemical bonding in the Si_5^{2-} species, which are compared with $B_5H_5^{2-}$. Even though Si_5 and Si_5^- have been extensively studied experimentally[19−50] and theoretically,[51−109] we included them in the current study for completeness and for better evaluation of the theoretical methods, which will be used to investigate larger multiply charged silicon clusters in the future.

† Part of the special issue "Jack Simons Festschrift".

* To whom correspondence should be addressed. E-mail: boldyrev@cc.usu.edu (A.I.B); ls.wang@pnl.gov (L.-S.W.)

10.1021/jp0526748 CCC: $30.25
Published on Web 09/30/2005

2. Experimental Methods

Details of the photoelectron spectroscopy (PES) apparatus have been described elsewhere.[110,111] Both the silicon cluster anions and Na−Si mixed cluster anions were generated by laser vaporization of a Si disk target and a Na/Si disk target in the presence of a helium carrier gas and analyzed by time-of-flight mass spectrometry. Either Si_5^- or $NaSi_5^-$ anions were mass-selected and decelerated before being photodetached by a pulsed laser beam. Photoelectrons were collected at nearly 100% efficiency by a magnetic bottle and analyzed in a 3.5 m long electron flight tube. The PES spectra were calibrated by using the known spectra of Au^-, Pt^-, and Rh^-, and the energy resolution was $\Delta E_k/E_k \approx 2.5\%$, that is, approximately 25 meV for 1 eV electrons.

3. Theoretical Methods

The initial search for the most stable structures was performed using our gradient embedded genetic algorithm (GEGA) program written by Alexandrova.[112] We used the semiempirical PM3 method for energy, gradient, and force calculations. The lowest few structures in every system were recalculated using a hybrid method known in the literature as B3LYP[113−115] with polarized split-valence basis sets (6-311+G*).[116−118] The lowest structure in every system was then refined using the coupled-cluster method with single, double, and noniterative triple excitations (CCSD(T))[119−121] with the same basis sets. Total energies of these structures were also calculated using the extended 6-311+G(2df) basis sets. Some species have been calculated using the second-order Møller−Plessett (MP2)[122] level of theory and the 6-311+G* basis sets. To test the validity of the one-electron approximation, single-point calculations were performed using the multiconfiguration self-consistent field method (CASSCF)[123,124] with eight and nine active electrons and seven active molecular orbitals for Si_5 and Si_5^-, respectively [CASSCF(8,7) and CASSCF(9,7)], and with 10 active electrons and eight active orbitals for Si_5^{2-} [CASSCF(10,8), all using 6-311+G* basis sets].

The vertical electron detachment energies (VDEs) were calculated using R(U)CCSD(T)/6-311+G(2df), the outer valence Green function method (OVGF/6-311+G(2df)),[125−129] and the equation of motion method based on the restricted coupled cluster method [EOM-CCSD(T)][130] at the CCSD(T)/6-311+G* geometries, as well as the time-dependent density functional theory method[131] (TD-B3LYP/6-311+G(2df)) at the B3LYP/6-311+G* geometries. VDEs were calculated as differences of total energies at the CCSD(T) level of theory. Corrections for electron correlation and relaxation were added directly to the one-electron molecular orbital (MO) energy in the OVGF method. VDEs were calculated in two steps at the TD-B3LYP and EOM-CCSD(T) levels of theory. Initially, the first VDE was calculated as a difference in total energies and then calculated vertical excitation energies for the system with one electron less were added to the first VDE to obtain second and higher VDEs. Core electrons were frozen in treating the electron correlation at the CCSD(T) and OVGF levels of theory.

Chemical bonding was analyzed using electron localization functions (ELFs).[132−134] All B3LYP, TD-B3LYP, CASSCF, UCCSD(T), and OVGF calculations were performed using Gaussian 98 and Gaussian 03 programs,[135] and RCCSD(T) and EOM-CCSD(T) calculations were performed using the MOLPRO-2000.1 program[136] on a 63-node Birch−Retford Beowulf cluster computer built at Utah State University by K. A. Birch, B. P. Retford, and E. Koyle. ELF calculations have been performed using the TopMod Package.[137] Visualization of ELFs has been made using the MOLEKEL program,[138] and molecular orbital visualization has been done using the MOLDEN3.4 program.[139]

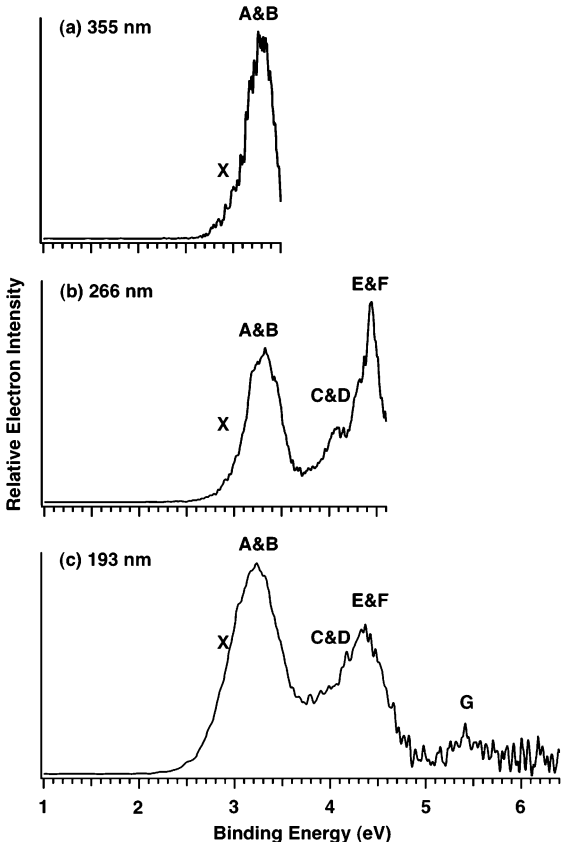

Figure 1. Photoelectron spectra of Si_5^- at (a) 355 nm (3.496 eV), (b) 266 nm (4.661 eV), and (c) 193 nm (6.424 eV).

4. Experimental Results

4.1. Photoelectron Spectroscopy of Si_5^-. Figure 1 shows the photoelectron spectra of Si_5^- at three photon energies (355, 266, and 193 nm). The photoelectron spectra of Si_5^- have been reported in a number of previous studies.[25,30,31,34,36] In particular, vibrationally resolved spectra have been obtained by Xu et al.[31] The current spectra agree with the previous data, but they provide better resolved features beyond 3.5 eV binding energies. The 355 nm spectrum (Figure 1a) displays a broad band with a low binding energy tail. From their vibrationally resolved spectra and angular dependent studies, Xu et al. showed that the 355 nm spectrum contained two electronic transitions, with the low-energy tail (X) corresponding to the ground-state transition. A long vibrational progression with an average spacing of 233 ± 10 cm^{-1} was observed in ref 31, suggesting a significant geometry change between the ground state of Si_5^- and Si_5. An adiabatic electron detachment energy (ADE) of 2.59 eV was estimated by Xu et al. from their Franck−Condon simulation. Thus the spectral onset at ~2.7 eV in the 355 nm spectrum only represents an upper limit for the ADE due to the large geometry changes between the anion and neutral ground state. The VDE of the X band is estimated to be around 3.0 eV, which is consistent with the Franck−Condon simulation by Xu et al. The intense part of the 355 nm spectrum at the high binding energy side (A) corresponds to the detachment transition to the first excited state of Si_5. The broad nature of the A band makes it difficult to evaluate its VDE, which should be approximately 3.2 eV.

TABLE 1: Experimental Compared with Calculated VDEs (eV) for D_{3h} ($^2A_2''$) Si_5^-

final state	expt	TD-B3LYP[a]	UOVGF[b]	CCSD(T)[c]	EOM[d]
$^1A_1'$ ($2a_1'^2 3a_1'^2 1e''^4 2e'^4 2a_2''^0$)	~3.0 (X)	3.06	2.99 (0.91)	3.01	3.01
$^3E''$ ($2a_1'^2 3a_1'^2 1e''^4 2e'^3 2a_2''^1$)	~3.2 (A)	3.13	2.95 (0.90)	3.24	*g*
$^1E''$ ($2a_1'^2 3a_1'^2 1e''^4 2e'^3 2a_2''^1$)	~3.4 (B)	3.52	*e*	*f*	3.26
$^3E'$ ($2a_1'^2 3a_1'^2 1e''^3 2e'^4 2a_2''^1$)	~4.1 (C)	4.03	3.87 (0.91)	*f*	*g*
$^1E'$ ($2a_1'^2 3a_1'^2 1e''^3 2e'^4 2a_2''^1$)	~4.3 (D)	4.36	*e*	*f*	4.50
$^3A_2''$ ($2a_1'^2 3a_1'^1 1e''^4 2e'^4 2a_2''^1$)	4.47 ± 0.03 (E)	4.29	4.31 (0.90)	*f*	*g*
$^1A_2''$ ($2a_1'^2 3a_1'^1 1e''^4 2e'^4 2a_2''^1$)	~4.6 (F)	4.52	*e*	*f*	4.81
$^3A_2''$ ($2a_1'^1 3a_1'^2 1e''^4 2e'^4 2a_2''^1$)	~5.4 (G)	5.27	4.92 (0.88)	*f*	*g*
$^1A_2''$ ($2a_1'^1 3a_1'^2 1e''^4 2e'^4 2a_2''^1$)		6.80	*e*	*f*	6.82

[a] The VDEs were calculated at the TD-B3LYP/6-311+G(2df)//B3LYP/6-311+G* level of theory. [b] The VDEs were calculated at the UOVGF/6-311+G(2df)//CCSD(T)/6-311+G* level of theory. The numbers in parentheses indicate the pole strength, which characterizes the validity of the one-electron-detachment picture. [c] The VDEs were calculated at the CCSD(T)/6-311+G(2df)//CCSD(T)/6-311+G* level of theory. [d] The VDEs were calculated at the CCSD(T)/6-311+G(2df)//CCSD(T)/6-311+G* level of theory. [e] The VDEs into the final singlet states were not calculated because of the multiconfigurational nature of the final singlet states. [f] The VDEs into these excited states cannot be calculated at this level of theory. [g] The VDEs into the final triplet states cannot be calculated using MOLPRO-2000-1.

The 266 nm spectrum (Figure 1b) indicates that the A band is cut off at 355 nm. This band in fact is shown to extent to around 3.6 eV, suggesting that there is likely to be another detachment transition. This is labeled as band B with a VDE at approximately 3.4 eV. As will be shown below, this band is borne out in the current theoretical calculations. Although it was not recognized at the time, the 299 nm spectrum in the paper by Xu et al.[31] resolved this band more clearly. The 266 nm spectrum (Figure 1b) reveals two more broad bands: a weak and broad band centered around 4 eV (C) and a more intense and sharper band at 4.47 eV (E). A shoulder can be discerned at the lower binding energy side of the intense band around 4.3 eV (D). At 193 nm (Figure 1c), band E becomes broad, suggesting an additional band around 4.6 eV, which is cut off in the 266 nm spectrum. A very weak band is also observed around 5.4 eV (G). We also took the spectrum of Si_5^- at 157 nm (not shown), but no new detachment transitions were observed because of the poor signal-to-noise ratio in the high binding energy side.

The VDEs of all the observed detachment channels for Si_5^- are summarized in Table 1, where the calculated VDEs at various levels of theory are also listed.

4.2. Photoelectron Spectroscopy of $NaSi_5^-$. The photoelectron spectra of $NaSi_5^-$ are shown in Figure 2 at three photon energies (355, 266, and 193 nm). The electron binding energies of $NaSi_5^-$ are lower than those of Si_5^-, but the overall spectral patterns for the two species are quite similar. The low binding energy part of the $NaSi_5^-$ spectra shows a very broad band, which also contains three overlapping detachment transitions (X, A, B) similar to the Si_5^- spectra. The VDE of the A band is assigned to be the most intense feature in this band at 2.67 eV in the 355 nm spectrum (Figure 2a). The X and B bands are assigned to be on the lower and higher binding energy sides of this broad band, and their binding energies are estimated to be ~2.55 and ~2.9 eV, respectively. The onset of the X band is relatively sharp for $NaSi_5^-$, allowing us to evaluate an ADE of 2.42 ± 0.04 eV, which agrees with the value of 2.45 ± 0.05 eV reported previously by Kishi et al. at 355 nm.[16] Following the broad band, three well-resolved bands are observed (C, D, E). Bands C and D with VDEs of 3.47 and 3.71 eV, respectively, are relatively weak, whereas band E at 3.95 eV is quite sharp and intense in the 266 nm spectrum (Figure 2b). At 193 nm (Figure 2c), the intensity of the E band is significantly reduced and a very weak band with a relatively poor signal-to-noise ratio is observed at ~5.5 eV (F). Overall the spectral features of $NaSi_5^-$ appear to be slightly sharper and better resolved than the Si_5^- counterparts, suggesting that the geometry changes between $NaSi_5^-$ and $NaSi_5$ are relatively small. All the observed

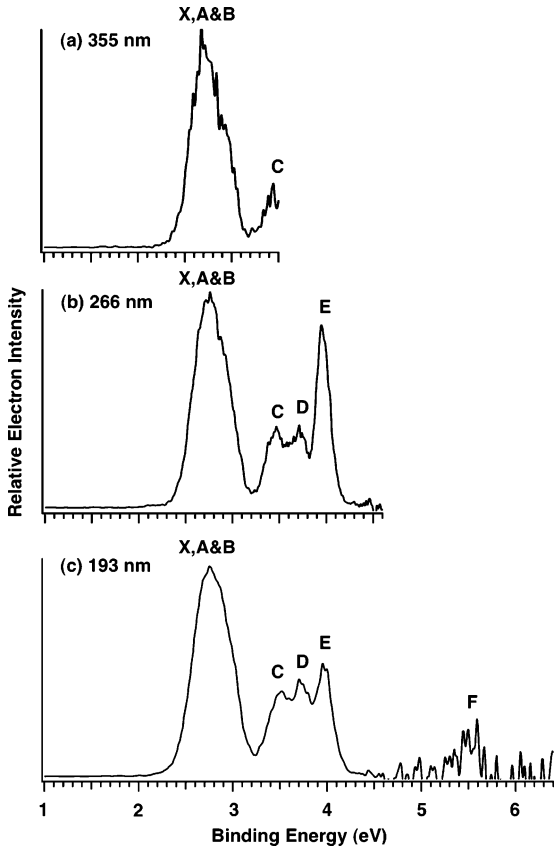

Figure 2. Photoelectron spectra of $NaSi_5^-$ at (a) 355 nm (3.496 eV), (b) 266 nm (4.661 eV), and (c)193 nm (6.424 eV).

VDEs for $NaSi_5^-$ are given in Table 2, where they are compared with theoretical calculations.

It has been demonstrated previously that PES combined with ab initio calculations is a powerful tool for elucidating the electronic structure and chemical bonding of novel clusters.[140] In the following, different levels of theory are employed to investigate the detailed structures and underlying chemical bonding of Si_5^- and $NaSi_5^-$ (Si_5^{2-}) and to assist the assignment of the observed photoelectron spectra.

5. Theoretical Results

The geometric structures of Si_5^{2-}, Si_5^-, and Si_5 are well established in the literature.[16,51−109] We performed the search for the global minimum structures for these species primarily to test our GEGA program. While the GEGA search could potentially be performed for these species at the B3LYP/3-21G

TABLE 2: Experimental Compared with Calculated VDEs (eV) for C_s (^{1}A′) $NaSi_5^-$

final state	expt	ROVGF[a]	TD-B3LYP[b]	UCCSD(T)[c]
^{2}A′ ($4a'^2 5a'^2 2a''^2 6a'^2 3a''^2 7a'^2 8a'^1$)	~2.55 (X)	2.47 (0.88)	2.52	2.54
^{2}A′ ($4a'^2 5a'^2 2a''^2 6a'^2 3a''^2 7a'^1 8a'^2$)	2.67 ± 0.04 (A)	2.68 (0.88)	2.59	*e*
^{2}A″ ($4a'^2 5a'^2 2a''^2 6a'^2 3a''^1 7a'^2 8a'^2$)	~2.9 (B)	2.90 (0.88)	2.74	*e*
^{2}A′ ($4a'^2 5a'^2 2a''^2 6a'^1 3a''^2 7a'^2 8a'^2$)	3.47 ± 0.04 (C)	3.29 (0.88)	3.40	*e*
^{2}A″ ($4a'^2 5a'^2 2a''^1 6a'^2 3a''^2 7a'^2 8a'^2$)	3.71 ± 0.04 (D)	3.73 (0.88)	3.43	*e*
^{2}A′ ($4a'^2 5a'^1 2a''^2 6a'^2 3a''^2 7a'^2 8a'^2$)	3.95 ± 0.03 (E)	3.83 (0.87)	3.74	*e*
^{2}A′ ($4a'^1 5a'^2 2a''^2 6a'^2 3a''^2 7a'^2 8a'^2$)	5.50 ± 0.06 (F)	5.83 (0.83)	5.66[d]	*e*

[a] The VDEs were calculated at the ROVGF/6-311+G(2df)//B3LYP6-311+G* level of theory. The numbers in parentheses indicate the pole strength, which characterizes the validity of the one-electron-detachment picture. [b] The VDEs were calculated at the TD-B3LYP/6-311+G(2df)//B3LYP/6-311+* level of theory. [c] The VDEs were calculated at the TD-CCSD(T)/6-311+G(2df)//B3LYP/6-311+G* level of theory. [d] The electron detachment becomes a strongly multiconfigurational process. [e] The VDEs into these excited states cannot be calculated at this level of theory.

level of theory, we used the semiempirical PM3 method for the energy, gradient, and force calculations. We plan to use the same level of theory for large silicon clusters, for which the B3LYP/3-21G GEGA calculations would not be possible with our computer resources.

5.1. Si_5^{2-}. The PM3 GEGA search yielded the bipyramidal D_{3h} ($^1A_1'$, $1a_1'^2 1a_2''^2 1e'^4 2a_1'^2 3a_1'^2 1e''^4 2e'^4 2a_2''^2$) global minimum structure I (Figure 3a). Two quasiplanar and planar isomers were also obtained: II, C_2 (^{1}A), and III, D_{2h} (^1A_g). We then performed B3LYP/6-311+G* geometry optimization and frequency calculations for structures I, II, and III. Again the global minimum structure at this level of theory was found to be structure I. We also performed CCSD(T)/6-311+G* calculations for structure I. Both geometric parameters and frequencies are in good agreement between the two methods, as shown in Table 3. Our optimized d_{eq-eq} (2.606 Å at B3LYP/6-311+G* and 2.591 Å at CCSD(T)/6-311+G*) and d_{ax-eq} (2.400 Å at B3LYP/6-311+G* and 2.389 Å at CCSD(T)/6-311+G*) values are slightly longer than the corresponding experimental values of $d_{eq-eq} = 2.535$ Å and $d_{ax-eq} = 2.350$ Å obtained in solid,[15] but they agree well with the ab initio calculations reported by Kishi et al.[16] The isomers II, C_{2v} ($^1A_1$), and III, D_{2h} (^1A_g), were found to be higher in energy than the global minimum structure by 37.0 and 41.3 kcal/mol (all at CCSD(T)/6-311+G(2df)//B3LYP/6-311+G*+ZPE correction at B3LYP/6-311+G*), respectively. Optimized geometry and harmonic frequencies calculated at the CASSCF(10,8)/6-311+G* level of theory are in good agreement with the results at B3LYP/6-311+G* and CCSD(T)/6-311+G* (Table 3). The Hartree−Fock configuration was found to be dominant ($C_{HF} = 0.943$) among 1176 configurations in the CASSCF wave function, thus confirming the applicability of the used one-electron configuration based methods. We also performed a single-point calculation with the extended active space CASSCF(12,9)/6-311+G*. The Hartree−Fock configuration was found to be almost the same ($C_{HF} = 0.943$) among 3570 configurations in the CASSCF wave function.

5.2. Si_5^- and Si_5. The similar PM3 GEGA search also yielded a bipyramidal D_{3h} ($^2A_2''$, $1a_1'^2 1a_2''^2 1e'^4 2a_1'^2 3a_1'^2 1e''^4 2e'^4 2a_2''^1$) global minimum structure for Si_5^- (IV, Figure 3d), with the lowest planar isomer VI being C_2 (^{2}B) (Figure 3f). Subsequent B3LYP/6-311+G* geometry optimization and frequency calculations for structures IV, V, and VI confirmed that structure IV (Table 4) is the global minimum. We also performed CCSD(T)/6-311+G* calculations for structure IV (Table 4). The D_{3h} ($^2A_2''$) global minimum structure was first predicted by Raghavachari[52] and has been confirmed in numerous calculations later.[16,51−64] Our PM3 GEGA findings and the more sophisticated calculations are in excellent agreement with the previous results. The lowest C_2 (^{2}B) isomer VI (Figure 3f) for Si_5^- found in our calculations is substantially higher in energy (by 30 kcal/mol at CCSD(T)/6-311+G(2df)//B3LYP/6-311+G*+ZPE corrections at B3LYP/6-311+G*) and thus should not be significantly populated in the Si_5^- ion beam.

For Si_5, our PM3 GEGA search revealed the bipyramidal D_{3h} ($^1A_1'$, $1a_1'^2 1a_2''^2 1e'^4 2a_1'^2 3a_1'^2 1e''^4 2e'^4 2a_2''^0$) global minimum structure VII (Figure 3g, Table 5) with a low-lying singlet C_{2v} ($^1A_1$) planar isomer VIII (Figure 3h). The bipyramidal D_{3h} global minimum for Si_5 was also first predicted by Raghavachari and Logovinsky[66] and has been confirmed by numerous subsequent calculations.[16,51,52,55,56,58−109] The lowest C_{2v} ($^1A_1$) isomer VIII (Figure 3h) for Si_5 was found to be substantially (28 kcal/mol at CCSD(T)/6-311+G(2df)//B3LYP/6-311+G*+ZPE corrections at B3LYP/6-311+G*) higher in energy.

We also optimized geometry and calculated harmonic frequencies at the CASSCF(9,7)/6-311+G* (Si_5^-) and CASSCF(8,7)/6-311+G* (Si_5) levels of theory (Tables 4 and 5). The CASSCF results are in good agreement with the results at B3LYP/6-311+G* and CCSD(T)/6-311+G*. The Hartree−Fock configurations were found to be dominant ($C_{HF} = 0.969$) among 490 configurations in the CASSCF wave function for Si_5^- and ($C_{HF} = 0.953$) among 490 configurations in the CASSCF wave function for Si_5, thus confirming the applicability of the one-electron configuration based methods.

5.3. $NaSi_5^-$. For the $NaSi_5^-$ anion we expected that the global minimum structure should be related to the trigonal-bipyramidal structure I of Si_5^{2-} (Figure 3a), because alternative structures for the dianion are substantially higher in energy. We placed a Na^+ cation at different positions around the D_{3h} Si_5^{2-}: (1) above a triangular face (Figure 3i), (2) above an edge between two equatorial Si atoms (Figure 3j), (3) above an edge between one axial and one equatorial Si atom (Figure 3k), (4) above an equatorial silicon atom (Figure 3l), and (5) above an axial Si atom (Figure 3m). Geometry optimization and frequency calculations for these structures were performed at the B3LYP/6-311+G* level of theory. The lowest energy structure among those is structure IX (C_s, ^{1}A′). This structure was reoptimized at the MP2/6-311+G* level of theory, and the results agree well with the B3LYP/6-311+G* results (Table 6). We were not able to converge geometry optimization at CCSD(T)/6-311+G* because of the numerical calculation procedure for gradients at the CCSD(T) level of theory and because of a very shallow potential energy surface. Structure X (C_{2v}, $^1A_1$), with the Na^+ cation located above the edge, was found to be a first-order saddle point at just 0.7 kcal/mol (CCSD(T)/6-311+G(2df)//B3LYP/6-311+G*+ZPE corrections at B3LYP/6-311+G*) above the global minimum. Thus, the $NaSi_5^-$ potential energy surface is very flat and the Na^+ cation can almost freely move from a position over the upper face to a position over the lower face in the Si_5^{2-} trigonal bipyramid. Structure XI (C_s, ^{1}A′) is also a first-order saddle point corresponding to internal motion of Na^+ around the upper or lower part of the Si_5^{2-} trigonal bipyramid. The barrier for this motion is appreciably higher (5.8

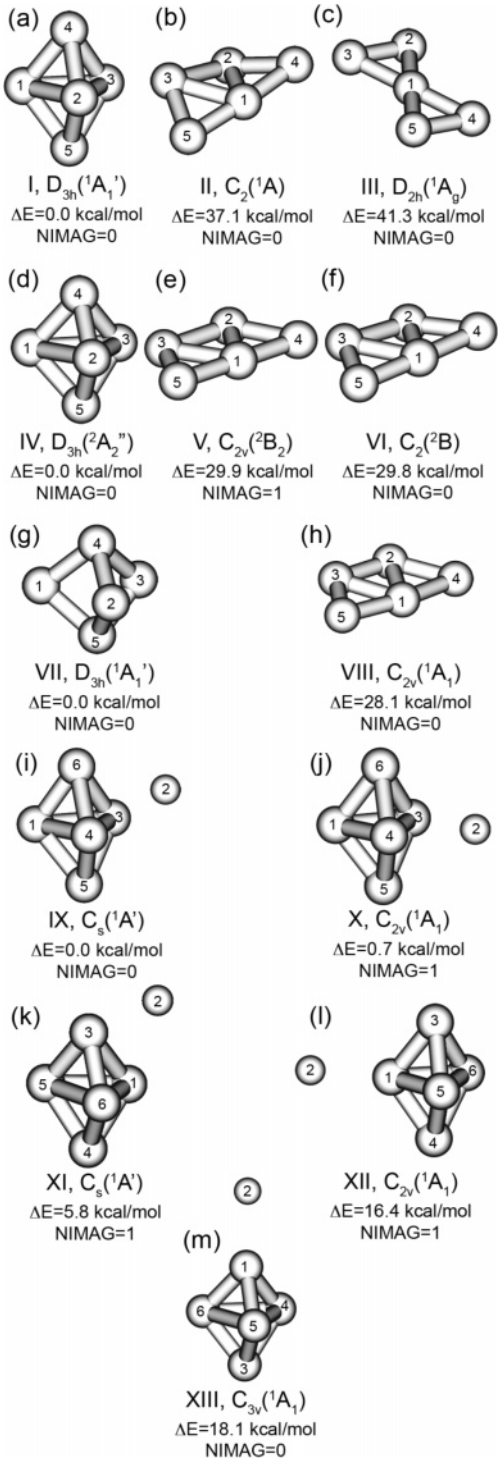

Figure 3. Optimized geometries (B3LYP/6-311+G*) of Si_5^{2-} (a−c), Si_5^- (d−f), Si_5 (g, h), and $NaSi_5^-$ (i−m). Relative energies are given at CCSD(T)/6-311+G(2df)//B3LYP/6-311+G*+ZPE. NIMAG, number of imaginary frequencies.

kcal/mol (CCSD(T)/6-311+G(2df)//B3LYP/6-311+G*+ZPE corrections at B3LYP/6-311+G*). Two other optimized structures with Na^+ coordinated to just one Si atom were found to be much higher in energy. Structure XII (C_{2v}, $^1A_1$) is a saddle point at B3LYP/6-311+G*, being 16.4 kcal/mol (CCSD(T)/6-311+G(2df)//B3LYP/6-311+G*+ZPE corrections at B3LYP/6-311+G*) higher in energy than the global minimum, and structure XIII (C_{3v}, $^1A_1$) is a local minimum, being 18.1 kcal/mol (CCSD(T)/6-311+G(2df)//B3LYP/6-311+G*+ZPE corrections at B3LYP/6-311+G*) above the global minimum.

TABLE 3: Calculated Molecular Properties of Si_5^{2-} D_{3h} ($^1A_1'$)

method	B3LYP/ 6-311+G*	CASSCF(10,8)/ 6-311+G*	CCSD(T)/ 6-311+G*
$-E$, au	1447.524 931	1444.582 724	1445.075 619
$R(Si_2-Si_5)$, Å	2.400	2.387	2.389
$R(Si_2-Si_3)$, Å	2.606	2.634	2.591
$\omega_1(a_1')$, cm^{-1}	432 (0.0)[a]	464	452
$\omega_2(a_1')$, cm^{-1}	332 (0.0)[a]	342	338
$\omega_3(a_2'')$, cm^{-1}	445 (1.3)[a]	485	457
$\omega_4(e')$, cm^{-1}	330 (0.0)[a]	341	336
$\omega_5(e')$, cm^{-1}	180 (0.9)[a]	190	176
$\omega_6(e'')$, cm^{-1}	301 (0.0)[a]	317	311

[a] Infrared intensities (km/mol) are given in parentheses.

TABLE 4: Calculated Molecular Properties of Si_5^- D_{3h} ($^2A_2''$)

method	B3LYP/ 6-311+G*	CASSCF(9,7)/ 6-311+G*	CCSD(T)/ 6-311+G*
$-E$, au	1447.581 738	1444.639 338	1445.139 672
$R(Si_2-Si_5)$, Å	2.356	2.348	2.346
$R(Si_2-Si_3)$, Å	2.778	2.730	2.751
$\omega_1(a_1')$, cm^{-1}	450 (0.0)[a]	480	467
$\omega_2(a_1')$, cm^{-1}	292 (0.0)[a]	310	306
$\omega_3(a_2'')$, cm^{-1}	428 (2.6)[a]	422	445
$\omega_4(e')$, cm^{-1}	360 (0.6)[a]	388	366
$\omega_5(e')$, cm^{-1}	192 (0.7)[a]	200	193
$\omega_6(e'')$, cm^{-1}	328 (0.0)[a]	333	345

[a] Infrared intensities (km/mol) are given in parentheses.

TABLE 5: Calculated Molecular Properties of Si_5 D_{3h} ($^1A_1'$)

method	B3LYP/ 6-311+G*	CASSCF(8,7)/ 6-311+G*	CCSD(T)/ 6-311+G*
$-E$, au	1447.492 144	1444.580 865	1445.060 178
$R(Si_2-Si_5)$, Å	2.330	2.330	2.316
$R(Si_2-Si_3)$, Å	3.125	3.173	3.073
$\omega_1(a_1')$, cm^{-1}	456 (0.0)[a]	474	477
$\omega_2(a_1')$, cm^{-1}	228 (0.0)[a]	216	239
$\omega_3(a_2'')$, cm^{-1}	375 (4.6)[a]	369	404
$\omega_4(e')$, cm^{-1}	432 (4.5)[a]	457	435
$\omega_5(e')$, cm^{-1}	170 (0.6)[a]	161	164
$\omega_6(e'')$, cm^{-1}	338 (0.0)[a]	323	364

[a] Infrared intensities (km/mol) are given in parentheses.

Even though the potential energy surface is very flat, our finding that the C_s ($^1A'$) structure IX is the global minimum for $NaSi_5^-$ disagrees with the conclusion of Kishi et al.,[16] who reported structure X with Na^+ coordinated to an equatorial edge as the global minimum.

6. Interpretation of the Photoelectron Spectra of Si_5^- and $NaSi_5^-$

6.1. Si_5^-. The VDEs of Si_5^- were calculated at four levels of theory (TD-B3LYP, UOVGF, CCSD(T), and EOM, all with 6-311+G(2df) basis sets), as summarized in Table 1. The VDEs calculated at the different levels of theory are surprisingly close to each other and agree with the experimental data very well. The ground-state transition corresponds to the electron detachment from the singly occupied $2a_2''$ HOMO, which is the same $2a_2''$ orbital in Si_5^{2-}, as shown in Figure 4a. This orbital is bonding within the equatorial atoms, but antibonding between the equatorial atoms and the axial atoms. Thus detachment of the $2a_2''$ electron leads to a considerable geometry change in neutral Si_5. It turns out that the largest change is in the equatorial Si−Si distances, which increase from 2.751 Å in Si_5^- to 3.073 Å in Si_5 accompanied by a very small contraction of the Si−Si distances between the equatorial and axial atoms (see Tables 4

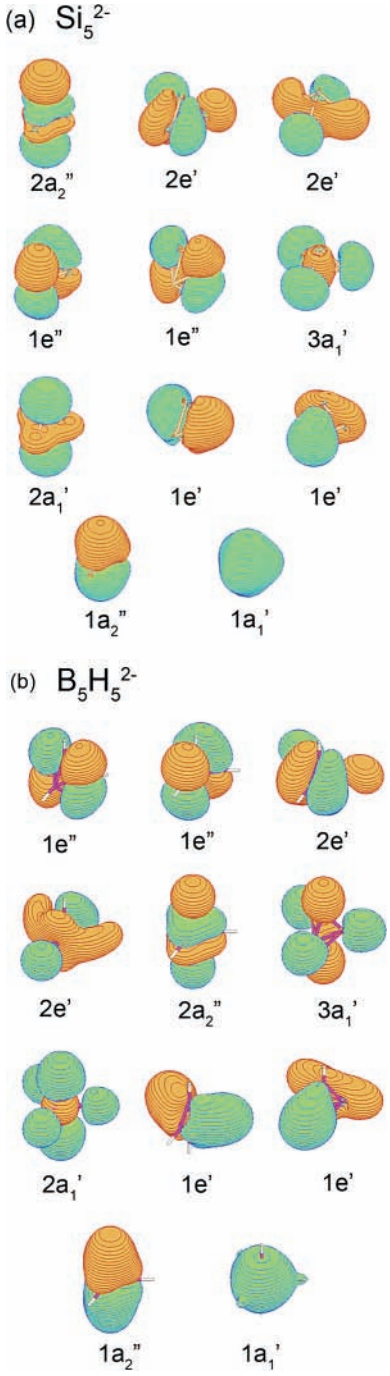

Figure 4. Valence molecular orbitals of (a) Si_5^{2-} (D_{3h}, $^1A_1'$) and (b) $B_5H_5^{2-}$ (D_{3h}, $^1A_1'$) at the RHF/6-311+G* level of theory.

and 5). The huge geometry changes lead to a very broad band for the ground-state transition. Xu et al. resolved a long vibrational progression for this transition with an average spacing of 233 cm^{-1}, which is in excellent agreement with our calculated frequency for the ν_1 mode (239 cm^{-1}, Table 5). Our calculated ADE, i.e., the adiabatic electron affinity of neutral Si_5, is 2.35 eV at B3LYP/6-311+G(2df) and 2.37 eV at CCSD(T)/6-311+G(2df), which is significantly lower than the calculated VDE (Table 1), consistent with the large geometry changes between the anion and neutral. The large geometry changes between Si_5^- and Si_5 mean that the ADE may not be obtained from the PES spectra because the Franck−Condon factor for the 0−0 transition may be negligible. Xu et al. estimated an ADE of 2.59 ± 0.02 eV from their Franck−Condon simulation.[31] Our observed detachment threshold in the 355 nm spectrum (Figure 1a) is around 2.7 eV. All of these should be viewed as upper limits for the ADE.

The next detachment is from the 2e′ HOMO−1 orbital, which can result in two detachment channels, a triplet and a singlet final state. These states are Jahn−Teller active and are expected to give very complicated spectral features. As given in Table 1, the calculated VDE for the triplet state ranges from 2.95 to 3.24 eV, whereas that for the singlet state ranges from 3.26 to 3.52 eV. These VDEs are in good agreement with the estimated VDEs for the overlapping A and B bands. Thus, the first broad feature (X, A, B) in the photoelectron spectra of Si_5^- contains three detachment transitions. From their vibrationally resolved data and angular dependent study, Xu et al. clearly resolved the A band. However, they did not recognize the third detachment channel corresponding to the singlet state ($^1E''$), even though they resolved it more clearly. The complex vibrational structures observed in their spectra agree with the Jahn−Teller effects expected for these final states.

The HOMO−2 orbital (1e″) is also a doubly degenerate MO. Detachment from this MO will again yield a triplet and a singlet state, which are Jahn−Teller active. The calculated VDE for the triplet state ranges from 3.87 to 4.03 eV, whereas that for the singlet state ranges from 4.36 to 4.50 eV. These calculated VDEs are in good agreement with the estimated VDEs for the C and D bands. The HOMO−3 is a nondegenerate orbital ($3a_1'$). Detachment from this orbital will also lead to a triplet state ($^3A_2''$) and a singlet state ($^1A_2''$). The calculated VDEs for these two states agree well with the estimated VDEs for the E and F bands, respectively.

Finally, the highest binding energy feature observed in the photoelectron spectra is the weak band G with an estimated VDE of ∼5.4 eV, which is in good agreement with the calculated VDE for the triplet final state from detachment from the $2a_1'$ HOMO−4 (Table 1). The calculated VDE for the corresponding singlet final state is about 6.8 eV. However, the intensity for this detachment channel is expected to be very low, considering the weak intensity for the triplet channel (G), and is not observed in the 157 nm spectrum, which also has very poor signal-to-noise ratios in the higher binding energy part. Overall, the calculated VDEs for the D_{3h} Si_5^- are in excellent agreement with the photoelectron spectra, confirming the D_{3h} structure for Si_5^- and lending credence for the TD-B3LYP and the UOVGF methods used to compute VDEs.

6.2. $NaSi_5^-$. The C_s $NaSi_5^-$ IX (Figure 3i) can be viewed as a D_{3h} Si_5^{2-} stabilized by a Na^+ cation. Si_5^{2-} is closed shell, and its 11 fully occupied valence MOs are shown in Figure 4a. Thus $NaSi_5^-$ is also closed shell and should give simpler photoelectron spectra because detachment from each occupied MO can only yield one doublet final state (Table 2). The HOMO of $NaSi_5^-$ is the 8a′ MO, which corresponds to the $2a_2''$ HOMO in Si_5^{2-} (Figure 4a). This is also the same HOMO in Si_5^-, albeit it is singly occupied in the latter. Detachment from the 8a′ HOMO of $NaSi_5^-$ yields the ground state of $NaSi_5$ [$Na^+(Si_5^-)$]. Even though the equatorial Si−Si bond lengths are shorter in Si_5^{2-} (Table 3) than in Si_5^- (Table 4), the change between Si_5^{2-} and Si_5^- (2.591 vs 2.751 Å) is only half that between Si_5^- and Si_5 (2.751 vs 3.073 Å). Thus the X band of $NaSi_5^-$ is sharper than that in the Si_5^- spectra. The calculated VDE for the ground-state transition at all three levels of theory (ROVGF, TD-B3LYP, and CCSD(T), all with 6-311+G(2df)) is in good agreement with the experiment.

The next two detachment channels correspond to the 7a′ and 3a″ orbitals, which can be traced to the pair of doubly degenerate 2e′ MO in Si_5^{2-} (Figure 4a). The Na^+ coordination to Si_5^{2-}

splits the degeneracy of the 2e′ orbitals. However, the calculated VDEs for these two MOs are fairly close to each other and they are also very close to the ground-state detachment channel. These three closely spaced detachment channels give rise to the broad band at the lower binding energies in the photoelectron spectra (X, A, and B in Figure 2 and Table 2). The photoelectron spectra of $NaSi_5^-$ at higher binding energies exhibit four well-separated bands (C, D, E, and F), which correspond to detachment from the 6a′, 2a″, 5a′, and 4a′ MOs, respectively. The calculated VDEs are all in excellent agreement with the experimental values (Table 2). The 6a′ and 2a″ MOs correspond to the 1e″ MO in Si_5^{2-}, whereas the 5a′ and 4a′ correspond to the $3a_1'$ and $2a_1'$ MOs of Si_5^{2-}, respectively (Figure 4a).

The overall agreement between the experimental spectral pattern and the calculated VDEs is very good, confirming the global minimum structure for $NaSi_5^-$ (C_s, $^1A'$), in which the Na^+ counterion is coordinated to the face of the trigonal-bipyramidal Si_5^{2-} (Figure 3i). Again, the two theoretical methods, ROVGF and TD-B3LYP, performed well for $NaSi_5^-$ and will be used in the future for large sodium coordinated silicon clusters.

7. Chemical Bonding in Si_5, Si_5^-, and Si_5^{2-}

Chemical bonding in Si_5 and Si_5^{2-} has been previously discussed.[77,81,141] In particular, Wang and Messmer,[77] and Patterson and Messmer,[81] have interpreted chemical bonding in Si_5 using the valence bond model, a key feature of which is that each atom is surrounded by a tetrahedrally oriented set of orbitals. Then, pairs of occupied orbitals are singlet spin coupled into electron pairs, which are spatially separated from one another due to the Pauli exclusion principle. For the Si_5 cluster they obtained six symmetry-equivalent bent bonds that arise from the overlap of two orbitals, one from each of two atoms. These six bonds describe 2e−2c bonding between axial and equatorial Si atoms. Every equatorial atom possesses a lone pair, and the two axial Si atoms form a long bond. According to this valence bond picture, the long bond is formed by two collinear tetrahedral orbitals on the two axial silicon atoms, which are pointing away from each other, but nevertheless overlap enough to form a bond. King et al.[141] pointed out that the trigonal-bipyramidal Si_5^{2-} is a three-dimensional aromatic cluster similar to the valence isoelectronic $B_5H_5^{2-}$ cluster on the basis of diatropic NICS(0) values: NICS(0) = −38.5 for Si_5^{2-} and NICS(0) = −25.9 for $B_5H_5^{2-}$. These dianions are also aromatic according to the *styx* Lipscomb rule,[11,12] and they also satisfy Wade's $2n + 2$ skeletal electron rule[142,143] for aromatic deltahedral systems. However, they do not obey Hirsch's $2(N + 1)^2$ rule[144] for three-dimensional aromaticity.

In our consideration of the chemical bonding in Si_5, Si_5^-, Si_5^{2-}, and $B_5H_5^{2-}$, we used the natural population analysis (NPA), molecular orbital analysis, electron localization functions (ELFs), and nuclear independent chemical shifts (NICS).

7.1. NPA Analysis. According to the NPA, an electron density change upon an electron detachment from Si_5^{2-} [$Q(Si_{eq}) = -0.40$ |e| (hybridization $3s^{1.63}3p^{2.71}$) and $Q(Si_{ax}) = -0.40$ |e| ($3s^{1.65}3p^{2.70}$)] to Si_5^- [$Q(Si_{eq}) = -0.20$ |e| ($3s^{1.68}3p^{2.48}$) and $Q(Si_{ax}) = -0.20$ |e| ($3s^{1.59}3p^{2.56}$)] occurs on all five atoms, while upon an electron detachment from Si_5^- to Si_5 [$Q(Si_{eq}) = +0.16$ |e| ($3s^{1.74}3p^{2.08}$) and $Q(Si_{ax}) = -0.24$ e ($3s^{1.59}3p^{2.60}$)] it occurs primarily on the equatorial Si atoms.

7.2. Molecular Orbital Analysis. The valence molecular orbital picture for $B_5H_5^{2-}$ is quite similar to that for Si_5^{2-} (Figure 4), although the order of their occupied MOs is somewhat different. This similarity at first glance indicates that the chemical skeletal bonding in the trigonal B_5 or Si_5 units should be quite similar. Indeed, King et al. calculated NICS(0) indices at the center of both dianions and reported that they are highly negative (−25.9 ppm for $B_5H_5^{2-}$ and −38.5 ppm for Si_5^{2-}), showing significant aromaticity in both species. The aromatic nature of deltahedral boranes has been previously discussed by King and Rouvray[145] and Aihara.[146]

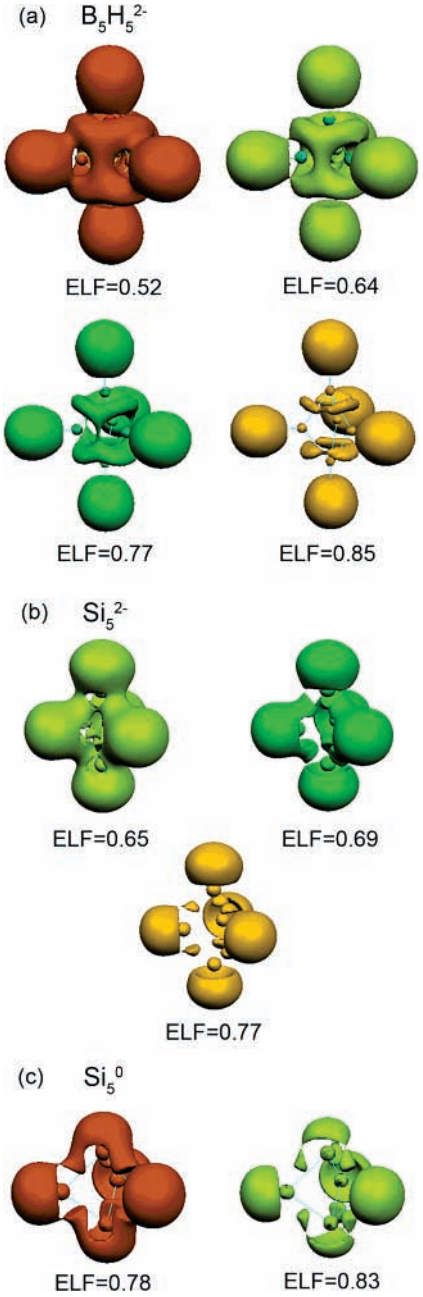

Figure 5. ELF bifurcations for (a) $B_5H_5^{2-}$ (D_{3h}, $^1A_1'$), (b) Si_5^{2-} (D_{3h}, $^1A_1'$), and (c) Si_5 (D_{3h}, $^1A_1'$) calculated at the B3LYP/6-311+G* level of theory.

7.3. ELF Analysis. The ELFs calculated for $B_5H_5^{2-}$, Si_5^{2-}, and Si_5 are presented in Figure 5. The local maxima of the ELFs define "localization attractors", of which there are only three basic types: bonding, nonbonding, and core. Bonding attractors lie between the core attractors (which themselves surround the atomic nuclei) and characterize the shared-electron interactions. The spatial organization of localization attractors provides a basis for a well-defined classification of bonds. From any point in space the ELF gradient is followed to an attractor in that region, and this point is then attributed to this attractor. The

collection of all the points in the space that is assigned to a given attractor is called its basin. The criterion of discrimination between basins is provided by the reduction of reducible (containing more than one attractor) domains. The reduction of a reducible localization domain occurs at critical values (saddle points) of the bonding isosurface, over which the domain is split into domains containing fewer attractors. The localization domains are then ordered with respect to the ELF critical values, yielding bifurcations.

The ELF pictures calculated for $B_5H_5^{2-}$ (Figure 5a) reveal that the protonated attractor domains (spherelike areas) are separated as a result of bifurcations at ELF = 0.52 (axial domains separated) and ELF = 0.64 (equatorial domains separated). These domains correspond to the 2e−2c B−H bonds. Two more bifurcations can be seen in Figure 5a at ELF = 0.77 and ELF = 0.85. The first bifurcation yields two reducible domains in the region of boron−boron bonding, and the second bifurcation reveals the six irreducible domains corresponding to six $B_{ax}-B_{eq}$ bonds. According to the ELF analysis, there is no $B_{eq}-B_{eq}$ bonding. This chemical bonding picture is consistent with the *styx* Lipscomb's description of chemical bonding in $B_5H_5^{2-}$.

The ELF pictures calculated for the valence isoelectronic Si_5^{2-} (Figure 5b) are somewhat different from those for the $B_5H_5^{2-}$ dianion. First, at ELF = 0.65 one can see the system of three attractors in the equatorial plane, which can be tentatively attributed to a pair of electrons delocalized in the equatorial area. At ELF = 0.69 one can see the separation of the two lone pairs corresponding to the axial Si atoms. Finally, at ELF = 0.77 one can see the separation of the three nonbonding domains corresponding to the equatorial Si atoms. Simultaneously, the six bonding domains corresponding to the $Si_{eq}-Si_{ax}$ bonds are revealed. Thus, in Si_5^{2-}, if compared to $B_5H_5^{2-}$, one can see that some electrons, which are supposed to belong to Si equatorial lone pairs, are actually participating in chemical skeletal bonding.

The bifurcations corresponding to the Si_5 neutral species are shown in Figure 5c. The major difference in the ELF analysis between Si_5 and Si_5^{2-} is the absence of the system of the three equatorial attractors in the neutral system and the significant alternation of the nonbonding domains corresponding to the axial Si atoms. It also should be pointed out that the interaction between the bonding $Si_{ax}-Si_{eq}$ domains and the axial nonbonding domains is appreciably stronger, because the bifurcation occurs at relatively high ELF values (0.69 for Si_5^{2-} and 0.83 for Si_5). Thus, the change in the electron density accompanying the removal of an electron pair from $Si_5^{2-} \rightarrow Si_5$ corresponds to the loss of electron density in the area primarily belonging to the equatorial Si atoms, and that is consistent with our NPA analysis discussed above.

7.4. NICS Analysis. We also performed calculations of the NICS indices (at B3LYP/6-311+G*) for Si_5^{2-}, Si_5^-, and Si_5 along the normal to the triangular face of the trigonal bipyramid starting from the center of the cluster. Our results are summarized in Table 7. We found that the NICS(0) values at the center of the cluster are highly negative for all the Si_5^{2-}, Si_5^-, and Si_5 species, clearly showing the presence of aromaticity in these clusters. The NICS(0) value increases along the Si_5^{2-}, Si_5^-, and Si_5 series. The NICS(0) value for the Si_5^{2-} dianion reported by King at al.[141] is very similar to our value. We found that the NICS value is growing along the normal for the Si_5^{2-} dianion and reaching the maximum value (−41.9 ppm) at the point of crossing the triangular face. That could be a manifestation of the additional contribution from the σ-aromaticity (aromaticity originated from the perpendicular $3p_x$ and $3p_y$ atomic orbitals of Si) in the triangular face of the trigonal bipyramid. When one electron is detached from the $2a_2''$ HOMO in Si_5^{2-}, the NICS values are substantially higher for almost all calculated points, but the NICS value at the point of crossing the triangular face is no longer the highest. Finally, when the second electron is removed from the $2a_2''$ HOMO in Si_5^{2-}, the NICS values are similar to those for Si_5^-, but now they are steadily decreasing from the center. These results show that, upon detachment of an electron pair from the $2a_2''$ HOMO in Si_5^{2-}, the contribution from σ-aromaticity in the neutral Si_5 is diminished.

TABLE 6: Calculated Molecular Properties of $NaSi_5^-$ C_s ($^1A'$)

method	B3LYP/6-311+G*	MP2/6-311+G*
$-E$, au	1609.923 210	1607.003 523
$R(Si_1-Si_{3,4})$, Å	2.519	2.487
$R(Si_1-Si_5)$, Å	2.438	2.400
$R(Si_1-Si_6)$, Å	2.353	2.344
$R(Si_3-Si_4)$, Å	2.698	2.638
$R(Si_5-Si_{3,4})$, Å	2.389	2.384
$R(Si_6-Si_{3,4})$, Å	2.456	2.439
$R(Na-Si_{3,4})$, Å	2.831	2.842
$R(Na-Si_5)$, Å	4.167	4.251
$R(Na-Si_6)$, Å	2.959	2.914
$\omega_1(a')$, cm^{-1}	446 (0.4)[a]	465 (2.4)[a]
$\omega_2(a')$, cm^{-1}	440 (1.1)[a]	459 (1.1)[a]
$\omega_3(a')$, cm^{-1}	344 (1.9)[a]	358 (0.7)[a]
$\omega_4(a')$, cm^{-1}	305 (5.9)[a]	342 (0.8)[a]
$\omega_5(a')$, cm^{-1}	294 (1.1)[a]	325 (3.6)[a]
$\omega_6(a')$, cm^{-1}	236 (24.9)[a]	244 (34.9)[a]
$\omega_7(a')$, cm^{-1}	185 (0.9)[a]	205 (1.3)[a]
$\omega_8(a')$, cm^{-1}	65 (7.0)[a]	87 (7.4)[a]
$\omega_9(a'')$, cm^{-1}	346 (1.7)[a]	365 (0.4)[a]
$\omega_{10}(a'')$, cm^{-1}	302 (0.1)[a]	336 (0.9)[a]
$\omega_{11}(a'')$, cm^{-1}	195 (5.4)[a]	193 (5.6)[a]
$\omega_{12}(a'')$, cm^{-1}	97 (1.1)[a]	89 (0.8)[a]

[a] Infrared intensities (km/mol) are given in parentheses.

TABLE 7: Calculated NICS (ppm) Indices for Si_5^{2-}, Si_5^-, and Si_5 at B3LYP/6-311+G*

position[a]	Si_5^{2-} (D_{3h},$^1A_1'$)	Si_5^- (D_{3h}, $^2A_2''$)	Si_5 (D_{3h}, $^1A_1'$)
0	−37.0	−48.9	−49.0
1	−37.9	−49.1	−48.8
2	−40.0	−49.4	−47.8
3[b]	−41.9	−48.2	−45.5
4	−41.4	−44.4	−41.0
5	−37.6	−37.9	−34.3

[a] NICS values are calculated along the normal to the triangular face of the trigonal bipyramid starting from the center of the cage. Increments are 0.233 Å for Si_5^{2-}, 0.242 Å for Si_5^-, and 0.256 Å for Si_5 clusters, respectively. [b] This point in the case of all three clusters corresponds to the intersection of the normal and the triangular face of the trigonal bipyramid.

8. Conclusions

We obtained photoelectron spectra for Si_5^- and $NaSi_5^-$ at several photon energies. The experimental spectra were interpreted by comparing with calculated VDEs at four different levels of theory (TD-B3LYP, R(U)OVGF, UCCSD(T), and EOM-CCSD(T), all with 6-311+G(2df) basis sets). Excellent agreement was found between the experiment and calculations for both anions, confirming their global minimum structures for Si_5^- (D_{3h}) and $NaSi_5^-$ (C_s). In the latter, Na^+ is coordinated to the face of a trigonal-pyramidal Si_5^{2-}. Chemical bonding in Si_5^{2-}, Si_5^-, Si_5, and $B_5H_5^{2-}$ was analyzed using NPA, molecular orbitals, ELF, and NICS indices. On the basis of these analyses we concluded that Si_5^{2-} differs from $B_5H_5^{2-}$ by involvement

of the electron density, which is supposed to be "lone pairs" in the skeletal bonding in Si_5^{2-}. The NICS indices indicated that all Si_5^{2-}, Si_5^-, and Si_5 clusters are highly aromatic. According to the higher negative NICS(0) value, the neutral and singly charged clusters are more aromatic than the doubly charged one.

Acknowledgment. The theoretical work done at Utah was supported by the National Science Foundation (CHE-0404937). The experimental work done at Washington was supported by the National Science Foundation (DMR-0503383) and performed at the W. R. Wiley Environmental Molecular Sciences Laboratory, a national scientific user facility sponsored by DOE's Office of Biological and Environmental Research and located at Pacific Northwest National Laboratory, which is operated for DOE by Battelle. D.Yu.Z. wishes to thank Utah State University for the Presidential Fellowship. The authors are grateful to Dr. A. Savin (University of Paris) for a fruitful discussion of the ELF results.

References and Notes

(1) Kroto, H. W.; Hearth, J. R.; O'Brien, S. C.; Curl, R. F.; Smalley, R. E. *Nature* **1985**, *318*, 162.
(2) Menon, M.; Subbaswamy, K. R. *Chem. Phys. Lett*. **1994**, *219*, 219.
(3) Gong, X. G.; Zheng, Q. Q. *Phys. Rev. B* **1995**, *52* (7), 4756.
(4) Song, J.; Ulloa, S. E.; Drabold, D. A. *Phys. Rev. B* **1996**, *53* (12), 8042.
(5) Li, B. X.; Jiang, M.; Cao, P. l. *J. Phys.: Condens. Matter* **1999**, *11*, 8517.
(6) Li, B. X.; Cao, P. L.; Que, D. L. *Phys. Rev. B* **2000**, *61* (3), 1685.
(7) Yu, D. K.; Zhang, R. Q.; Lee, S. T. *Phys. Rev. B* **2002**, *65*, 245417.
(8) Chen, Z.; Jiao, H.; Seifert, G.; Horn, A. H. C.; Yu, D.; Clark, T.; Thiel, W.; Schleyer, P. v. R. *J. Comput. Chem*. **2003**, *24*, 948.
(9) Sun, Q.; Wang, Q.; Jena, P.; Rao, B. K.; Kawazoe, Y. *Phys. Rev. Lett*. **2003**, *90* (13), 135503.
(10) Jemmis, E. D.; Prasad, B. V.; Tsuzuki, S.; Tanabe, K. *J. Phys. Chem*. **1990**, *94*, 5530.
(11) Lipscomb, W. N. *Boron Hydrides*; Benjamin: New York, 1963.
(12) Muetterties, E. L. *Boron Hydride Chemistry*; Academic Press: New York, 1975.
(13) Cotton, F. A.; Wilkinson, G.; Murillo, C. A.; Bochmann, M. *Advanced Inorganic Chemistry*, 6th ed.; Wiley-Interscience: New York, 1999.
(14) Zubarev, D. Yu.; Boldyrev, A. I. Unpublished results.
(15) Goicoechea, J. M.; Sevov, S. C. *J. Am. Chem. Soc*. **2004**, *126*, 6860.
(16) Kishi, R.; Kawamata, H.; Negishi, Y.; Iwata, S.; Nakajima, A.; Kaya, K. *J. Chem. Phys*. **1997**, *107*, 10029.
(17) Li, S.-D.; Guo, Q.-L.; Zhao, X.-F.; Wu, H.-S.; Jin, Z.-H. *J. Chem. Phys*. **2002**, *117*, 606.
(18) Li, S.-D.; Ren, G.-M.; Jin, Z.-H. *J. Chem. Phys*. **2003**, *119*, 10063.
(19) Bloomfield, L. A.; Geusic, M. E.; Freeman, R. R.; Brown, W. L. *Chem. Phys. Lett*. **1985**, *121*, 33.
(20) Reents, W. D., Jr.; Bondybey, V. E. *Chem. Phys. Lett*. **1986**, *125*, 324.
(21) Mandich, M. L.; Reents, W. D., Jr.; Bondybey, V. E. *J. Phys. Chem*. **1986**, *90*, 2315.
(22) Reents, W. D., Jr.; Mandich, M. L.; Bondybey, V. E. *Chem. Phys. Lett*. **1986**, *131*, 1.
(23) Liu, Y.; Zhang, Q. L.; Tittel, F. K.; Curl, R. F.; Smalley, R. E. *J. Chem. Phys.* **1986**, *85*, 7434.
(24) Mandich, M. L.; Bondybey, V. E.; Reents, W. D., Jr. *J. Phys. Chem*. **1987**, *86*, 4245.
(25) Chesnovsky, O.; Yang, S. H.; Pettiette, C. L.; Craycraft, M. J.; Liu, Y.; Smalley, R. E. *Chem. Phys. Lett*. **1987**, *138*, 119.
(26) Mandich, M. L.; Reents, W. D., Jr. *J. Chem. Phys*. **1989**, *90*, 3121.
(27) Mandich, M. L.; Reents, W. D., Jr.; Kolenbrander, K. D. *Pure Appl. Chem*. **1990**, *62*, 1653.
(28) John, P. M. St.; Whetten, R. L. *Chem. Phys. Lett*. **1992**, *196*, 330.
(29) Terasaki, A.; Yamaguchi, H.; Yasumatsu, H.; Kondow, T. *Chem. Phys. Lett*. **1996**, *262*, 269.
(30) Kaya, K.; Nakajima, A. *Mater. Sci. Eng., A* **1996**, *217/218*, 7.
(31) Xu, C.; Taylor, T. R.; Burton, G. R.; Neumark, D. M. *J. Chem. Phys*. **1998**, *108* (4), 1395.
(32) Muller, J.; Liu, B,; Shvartsburg, A. A.; Ogut, S.; Chelikowsky, J. R.; Siu, K. W. M.; Ho, K. M.; Gantefor, G. *Phys. Rev. Lett*. **2000**, *85*, 1666.
(33) Shvartsburg, A. A.; Hudgins, R. R.; Dugourd, P.; Jarrold, M. F. *Chem. Soc. Rev*. **2001**, *30*, 26.
(34) Hoffmann, M. A.; Wrigge, G.; Issendorff, B. v.; Muller, J.; Gantefor, G.; Haberland, H. *Eur. Phys. J. D* **2001**, *16*, 9.
(35) Bergeron, D. E.; Castleman, A. W., Jr. *J. Chem. Phys*. **2002**, *117*, 3219.
(36) Kronik, L.; Fromherz, R.; Ko, E.; Gantefor, G.; Chelikowsky, J. R. *Eur. Phys. J. D* **2003**, *24*, 33.
(37) Yasumatsu, H.; Kondow, T. *Rep. Prog. Phys.* **2003**, *66*, 1783.
(38) Heath, J. R.; Liu, Y.; O'Brien, S. C.; Zhang, Q. L.; Curl, R. F.; Tittel, F. K.; Smalley, R. E. *J. Chem. Phys.* **1985**, *83*, 5520.
(39) Creasy, W. R.; O'Keefe, A.; McDonald, J. R. *J. Phys. Chem*. **1987**, *91*, 2848.
(40) Zhang, Q. L.; Liu, Y.; Curl, R. F.; Tittel, F. K.; Smalley, R. E. *J. Chem. Phys.* **1988**, *88*, 1670.
(41) Jarrold, M. F.; Bower, J. E. *J. Phys. Chem.* **1988**, *92*, 5702.
(42) Beck, S. M.; Andrews, J. M. *J. Chem. Phys.* **1989**, *91*, 4420.
(43) Jarrold, M. F.; Honea, E. C. *J. Phys. Chem.* **1991**, *95*, 9181.
(44) Fuke, K.; Tsukamoto, K.; Misaizu, F.; Sanekata, M. J. *J. Chem. Phys*. **1993**, *99*, 7807.
(45) Ran, Q.; Schmude, R. W., Jr.; Miller, M.; Gingerich, K. A. *Chem. Phys. Lett*. **1994**, *230*, 337.
(46) Li, S.; Van Zee, R. J.; Weltner, W., Jr.; Raghavachari, K. *Chem. Phys. Lett*. **1995**, *243*, 275.
(47) Honea, E. C.; Ogura, A,; Peale, D. R.; Felix, C.; Murray, C. A.; Raghavachari, K.; Sprenger, W. O.; Jarrold, M. F.; Brown, W. L. *J. Chem. Phys.* **1999**, *110*, 12161.
(48) Patrone, L.; Ozerov, I.; Sentis, M. L.; Marine, W. *J. Phys. IV* **2001**, *11*, 121.
(49) Bulgakov, A. V.; Ozerov, I.; Marine, W. *Appl. Phys., A* **2004**, *79* (4−6), 1591.
(50) Bulgakov, A. V.; Ozerov, I.; Marine, W. *Thin Solid Films* **2004**, *453−454*, 557.
(51) Tomanek, D.; Schluter, M. A. *Phys. Rev. B* **1987**, *36*, 1208.
(52) Raghavachari, K. *Z. Phys. D* **1989**, *12*, 61.
(53) Raghavachari, K.; Rohlfing, C. M. *J. Chem. Phys*. **1991**, *94*, 3670.
(54) Adamowicz, L. *Chem. Phys. Lett*. **1992**, *188*, 131.
(55) Curtiss, L. A.; Deutsch, P. W.; Raghavachari, K. *J. Chem. Phys*. **1992**, *96*, 6868.
(56) Binggeli, N.; Martins, J. L.; Chelikowsky, J. R. *Phys. Rev. Lett*. **1992**, *68*, 2956.
(57) Binggeli, N.; Chelikowsky, J. R. *Phys. Rev. Lett*. **1995**, *75*, 493.
(58) Wei, S.; Barnett, R. N.; Landman, U. *Phys. Rev. B* **1997**, *55*, 7935.
(59) Kishi, R.; Iwata, S.; Nakajima, A.; Kaya, K. *J. Chem. Phys*. **1997**, *107*, 3056.
(60) Kishi, R.; Negishi, Y.; Kawamata, H.; Iwata, S.; Nakajima, A.; Kaya, K. *J. Chem. Phys*. **1998**, *108*, 8039.
(61) Shvartsburg, A. A.; Liu, B.; Jarrold, M. F.; Ho, K. M. *J. Chem. Phys.* **2000**, *112*, 4517.
(62) Zhao, C.; Balasubramanian, K. *J. Chem. Phys*. **2002**, *116*, 3690.
(63) Li, B. X.; Cao, P. L.; Song, B.; Ye, Z. Z. *Phys. Lett. A* **2003**, *307*, 318.
(64) Ishii, S.; Ohno, K.; Kumar, V.; Kawazoe, Y. *Phys. Rev. B* **2003**, *68*, 195412.
(65) Weinert, C. M. *Surf. Sci.* **1985**, *156*, 641.
(66) Raghavachari, K.; Logovinsky, V. *Phys. Rev. Lett*. **1985**, *55*, 2853.
(67) Tomanek, D.; Schluter, M. A. *Phys. Rev. Lett*. **1986**, *56*, 1055.
(68) Pacchioni, G.; Koutecky, J. *J. Chem. Phys*. **1986**, *84*, 3301.
(69) Raghavachari, K. *J. Chem. Phys*. **1986**, *84*, 5672.
(70) Feuston, B. P.; Kalia, R. K.; Vashishta, P. *Phys. Rev. B* **1987**, *35*, 6222.
(71) Andreoni, W.; Ballone, P. *Phys. Scr., T* **1987**, *T19*, 289.
(72) Raghavachari, K.; Rohlfing, C. M. *Chem. Phys. Lett*. **1988**, *143*, 428.
(73) Raghavachari, K.; Rohlfing, C. M. *J. Chem. Phys*. **1988**, *89*, 2219.
(74) Chelikowsky, J. R.; Phillips, J. C.; Kamal, M.; Strauss, M. *Phys. Rev. Lett*. **1989**, *62*, 292.
(75) Tomanek, D.; Sun, C.; Sharma, N.; Wang, L. *Phys. Rev. B* **1989**, *39*, 5361.
(76) Chelikowsky, J. R.; Phillips, J. C. *Phys. Rev. B* **1990**, *41*, 5735.
(77) Wang, H. X.; Messmer, R. P. *Phys. Rev. B* **1990**, *41*, 5306.
(78) Rohlfing, C. M.; Raghavachari, K. *Chem. Phys. Lett*. **1990**, *167*, 559.
(79) Andreoni, W.; Pastore, G. *Phys. Rev. B* **1990**, *41*, 10243.
(80) Sankey, O. F.; Niklewski, D. J.; Drabold, D. A.; Dow, J. D. *Phys. Rev. B* **1990**, *41*, 12750.
(81) Patterson, C. H.; Messmer, R. P. *Phys. Rev. B* **1990**, *42*, 7530.
(82) Chelikowsky, J. R.; Glassford, K. M.; Phillips, J. C. *Phys. Rev. B* **1991**, *44*, 1538.
(83) Salk, S. H. S.; Lutrus, C. K.; Hagen, D. E.; Oshiro, T.; Beck, S.; Loper, G. L. *Phys. Rev. B* **1992**, *45*, 1458.
(84) Fournier, R.; Sinnott, S. B.; DePristo, A. E. *J. Chem. Phys*. **1992**, *97*, 4149.
(85) Niessen, W. v.; Zakrzewski, V. G. *J. Chem. Phys.* **1993**, *98*, 1271.

(86) Lee, I. H.; Chang, K. J.; Lee, Y. H. *J. Phys.: Condens. Matter* **1994**, *6*, 741.
(87) Mittelbach, v. T.; Fritsche, H. G.; Muller, H. *Z. Phys. Chem*. **1994**, *187*, 45.
(88) Zhao, J.; Chen, X.; Sun, Q.; Liu, F.; Wang, G. *Phys. Lett. A* **1995**, *198*, 243.
(89) Govind, N.; Mozos, J. L.; Guo, H. *Phys. Rev. B* **1995**, *51*, 7101.
(90) Ramakrishna, M. V.; Bahel, A. *J. Chem. Phys*. **1996**, *104*, 9833.
(91) Jackson, K.; Pederson, M. R.; Porezag, D.; Hajnal, Z.; Frauenheim, T. *Phys. Rev. B* **1997**, *55*, 2549.
(92) Ho, K. M.; Shvartsburg, A. A.; Pan, B.; Lu, Z. Y.; Wang, C. Z.; Wacker, J. G.; Fye, J. L.; Jarrold, M. F. *Nature* **1998**, *392*, 582.
(93) Shvartsburg, A. A.; Jarrold, M. F.; Liu, B.; Lu, Z. Y.; Wang, C. Z.; Ho, K. M. *Phys. Rev. Lett.* **1998**, *81*, 4616.
(94) Liu, B.; Lu, Z. Y.; Pan, B.; Wang, C. Z.; Ho, K. M. *J. Chem. Phys.* **1998**, *109*, 9401.
(95) Qiu, M.; Jiang, M.; Zhao, Y. J.; Cao, P. L. *J. Chem. Phys.* **1999**, *110*, 10738.
(96) Lu, Z. Y.; Wang, C. Z.; Ho, K. M. *Phys. Rev. B* **2000**, *61*, 2329.
(97) Iwamatsu, M. *J. Chem. Phys.* **2000**, *112*, 10976.
(98) Li, B. X.; Cao, P. L. *J. Phys.: Condens. Matter* **2000**, *12*, 8357.
(99) Li, B. X.; Cao, P. L. *Phys. Rev. B* **2000**, *62*, 15788.
(100) Panda, B. K.; Mukherjee, S.; Behera, S. N. *Phys. Rev. B* **2001**, *63*, 045404.
(101) Li, B. X.; Cao, P. L.; Ye, Z.; Zhang, R. Q.; Lee, S. T. *J. Phys.: Condens. Matter* **2002**, *14*, 1723.
(102) Zhu, X.; Zeng, X. C. *J. Chem. Phys*. **2003**, *118*, 3558.
(103) Maroulis, G.; Begue, D.; Pouchan, C. *J. Chem. Phys*. **2003**, *119*, 794.
(104) Yoo, S.; Zeng, X. C. *J. Chem. Phys.* **2003**, *119*, 1442.
(105) Tekin, A.; Hartke, B. *Phys. Chem. Chem. Phys.* **2004**, *6*, 503.
(106) Pouchan, C.; Begue, D.; Zhang, D. Y. *J. Chem. Phys*. **2004**, *121*, 4628.
(107) Nigam, S.; Majumder, C.; Kulshreshtha, S. K. *J. Chem. Phys.* **2004**, *121*, 7756.
(108) Majumder, C.; Kulshreshtha, S. K. *Phys. Rev. B* **2004**, *69*, 115432.
(109) Nair, N. N.; Bredow, T.; Jug, K. *J. Comput. Chem*. **2004**, *25*, 1255.
(110) Wang, L. S., Wu, H. Probing the electronic structure of transition metal clusters from molecular to bulk-like using photoelectron spectroscopy. In *Advances in Metal and Semiconductor Clusters. IV. Cluster Materials*; Duncan, M. A., Ed.; JAI Press: Greenwich, CT, 1998; pp 299−343.
(111) Wang, L. S.; Cheng, H. S.; Fan, J. *J. Chem. Phys.* **1995**, *102*, 9480.
(112) (a) Alexandrova, A. N.; Boldyrev, A. I.; Fu, Y.-J.; Wang, X.-B.; Wang, L.-S. *J. Chem. Phys*. **2004**, *121*, 5709. (b) Alexandrova, A. N.; Boldyrev, A. I. *J. Chem. Theory Comput.* **2005**, *1*, 566.
(113) Parr, R. G.; Yang, W. *Density-functional theory of atoms and molecules*; Oxford University Press: Oxford, 1989.
(114) Becke, A. D. *J. Chem. Phys*. **1993**, *98*, 5648.
(115) Perdew, J. P.; Chevary, J. A.; Vosko, S. H.; Jackson, K. A.; Pederson, M. R.; Singh, D. J.; Fiolhais, C. *Phys. Rev. B* **1992**, *46*, 6671.
(116) McLean, A. D.; Chandler, G. S. *J. Chem. Phys.* **1980**, *72*, 5639.
(117) Clark, T.; Chandrasekhar, J.; Spitznagel, G. W.; Schleyer, P. v. R. *J. Comput. Chem.* **1983**, *4*, 294.
(118) Frisch, M. J.; Pople, J. A.; Binkley, J. S. *J. Chem. Phys.* **1984**, *80*, 3265.
(119) Cizek, J. *Adv. Chem. Phys.* **1969**, *14*, 35.
(120) Knowles, P. J.; Hampel, C.; Werner, H.-J. *J. Chem. Phys*. **1993**, *99*, 5219.
(121) Raghavachari, K.; Trucks, G. W.; Pople, J. A.; Head-Gordon, M. *Chem. Phys. Lett.* **1989**, *157*, 479.
(122) Head-Gordon, M.; Pople, J. A.; Frisch, M. J. *Chem. Phys. Lett*. **1988**, *153*, 503.
(123) Bernardi, F.; Bottini, A.; McDougall, J. J. W.; Robb, M. A.; Schlegel, H. B. *Faraday Symp. Chem. Soc*. **1979**, *19*, 137.
(124) Frisch, M. J.; Ragazos, I. N.; Robb, M. A.; Schlegel, H. B. *Chem. Phys. Lett*. **1992**, *189*, 524.
(125) Cederbaum, L. S. *J. Phys B* **1975**, 8, 290.
(126) von Niessen, W.; Shirmer, J.; Cederbaum, L. S. *Comput. Phys. Rep.* **1984**, *1*, 57.
(127) Zakrzewski, V. G.; von Niessen, W. *J. Comput. Chem.* **1993**, *14*, 13.
(128) (a) Ortiz, J. V. *Int. J. Quantum Chem., Quantum Chem. Symp*. **1989**, *23*, 321. (b) Lin, J. S.; Ortiz, J. V. *Chem. Phys. Lett*. **1990**, *171*, 197.
(129) Zakrzewski, V. G.; Ortiz, J. V.; Nichols, J. A.; Heryadi, D.; Yeager, D. L.; Golab, J. T. *Int. J. Quantum Chem. Symp.* **1996**, *60*, 29.
(130) (a) Werner, H.-J.; Knowles, P. J. *J. Chem. Phys*. **1988**, *89*, 5803. (b) Knowles, P. J.; Werner, H.-J. *Chem. Phys. Lett.* **1988**, *145*, 514.
(131) (a) Bauernshmitt, R.; Alrichs, R. *Chem. Phys. Lett.* **1996**, *256*, 454. (b) Casida, M. E.; Jamorski, C.; Casida, K. C.; Salahub, D. R. *J. Chem. Phys*. **1998**, *108*, 4439.
(132) Becke, A. D.; Edgecombe, K. E. *J. Chem. Phys*. **1990**, *92*, 5397.
(133) Savin, A.; Silvi, B.; Colonna, F. *Can. J. Chem*. **1996**, *74*, 1088.
(134) Savin, A.; Nesper, R.; Wengert, S.; Fassler, T. F. *Angew. Chem., Int. Ed. Engl*. **1997**, *36*, 1808.
(135) (a) Frisch, M. J.; et al. *Gaussian 98*, revision A.7; Gaussian, Inc.: Pittsburgh, PA, 1998. (b) Frisch, M. J.; et al. *Gaussian 03*, version B. 02; Gaussian, Inc.: Pittsburgh, PA, 2003.
(136) Werner, H.-J.; Knowles, P. J. With contributions from: Amos, R. D.; Bernhardsson, A.; Berning, A.; Celani, P.; Cooper, D. L.; Deegan, M. J. O.; Dobbyn, A. J.; Eckert, F.; Hampel, C.; Hetzer, G.; Korona, T.; Lindh, R.; Lloyd, A. W.; McNicholas, S. J.; Manby, F. R.; Meyer, W.; Mura, M. E.; Nicklass, A.; Palmieri, P.; Pitzer, R.; Rauhut, G.; Schutz, M.; Stoll, H.; Stone, A. J.; Tarroni, R.; Thorsteinsson, T. *MOLPRO-2000.1*.
(137) Noury, S.; Krokidis, X.; Fuster, F.; Silvi, B. *TopMod Package*; Universite Pierre et Marie Curie, 1997. Noury, S.; Krokidis, X.; Fuster, F.; Silvi, B. *Comput. Chem*. **1999**, *23*, 597.
(138) *MOLEKEL*, version 4.3; Stefan Portmann, CSCS/ETHZ, 2002.
(139) Schaftenaar, G. *MOLDEN3.4*; CAOS/CAMM Center, The Netherlands, 1998.
(140) Boldyrev, A. I.; Wang, L.-S. *J. Phys. Chem. A* **2001**, *105*, 10759.
(141) King, B. R.; Heine, T.; Corminboeuf, C.; Schleyer, P. v. R. *J. Am. Chem. Soc*. **2004**, *126*, 430.
(142) Wade, K. *Chem. Commun*. **1971**, 792.
(143) Wade, K. *Adv. Inorg. Chem. Radiochem*. **1976**, *18*, 1.
(144) Hirsch, A.; Chen, Z.; Jiao, H. *Angew. Chem., Int. Ed*. **2001**, *40*, 2834.
(145) King, R. B.; Rouvray, D. H. *J. Am. Chem. Soc*. **1977**, *99*, 7834.
(146) Aihara, J. J. *J. Am. Chem. Soc*. **1978**, *100*, 3339.